Acta Materialia 196 (2020) 252–260

Contents lists available at ScienceDirect

Acta Materialia

journal homepage: www.elsevier.com/locate/actamat

Full length article

# Cyclic strain amplitude-dependent fatigue mechanism of gradient nanograined Cu

Q.S. Pan, J.Z. Long, L.J. Jing, N.R. Tao, L. Lu*

*Shenyang National Laboratory for Materials Science, Institute of Metal Research, Chinese Academy of Sciences, Shenyang 110016, PR China*

ARTICLE INFO

*Article history:*
Received 24 February 2020
Revised 8 June 2020
Accepted 24 June 2020
Available online 30 June 2020

*Keywords:*
Gradient nanograin (GNG)
Cyclic response
Grain coarsening
Strain delocalization
Fatigue mechanism

ABSTRACT

Different grain coarsening behaviors (i.e. abnormal and homogeneous) are prevalently observed in gradient nanograined (GNG) Cu under stress controlled high-cycle and strain controlled low-cycle fatigue tests, respectively. In this paper, to comprehensively understand the intrinsic fatigue mechanism of gradient nanograined structures, both high and low cycle fatigue behaviors of GNG Cu are investigated under strain-controlled fatigue tests with a wide strain amplitude ranges. Cyclic behavior transition from abnormal grain coarsening at small strain amplitude to homogeneous grain coarsening at large strain amplitude is observd in GNG Cu. Microstrucural analysis reveals that the grain coarsening behavior in either abnormal or normal (homogeneous) mode is closely related to the spatial distribution of the cyclic plastic strain in the GNG layer (localized or delocalized) under cyclic loading. Such unique cyclic strain amplitude-dependent fatigue behavior is inherent to the gradient nanostructure, which fundamentally differs from the conventional strain localizing mechanism in metals with homogeneous structures under cyclic loading.



## 1. Introduction

Homogeneously refining grains of metals and alloys into ultrafine (UFG) or nanoscale (NG) can make them several times stronger in strength and hardness, compared to coarse grained (CG) counterparts, exhibiting a broad potential for engineering applications [1–3]. However, under cyclic loading condition in service, shorter strain controlled low-cycle fatigue life [4–6] and slightly enhanced stress-controlled high-cycle fatigue limit (i.e. very low fatigue limit/strength ratio, ~0.2) [7–9] are universally observed in a variety of UFG and NG metals and alloys. Most seriously, they experience severe cyclic softening with rapidly reduced stress amplitude with increasing fatigue cycles [4, 10–13]. This is primarily attributed to cyclic strain localization in the unstable nanostructures, i.e. abnormal grain coarsening and/or microscopically shear banding, under either strain or stress control, irrespective of the imposed stress/strain amplitudes [5, 10, 14–21].

Previous studies suggest that bimodal structure with CG randomly distributed in UFG matrix can enhance strain-controlled fatigue life to some extent, but exhibits cyclic softening and a very low fatigue limit comparable to CG, owing to strain localization and cracking in CG interiors [22, 23]. How to suppress the cyclic strain localization and further improve failure resistance of high-strength nanostructured metals has thus become a challenge in the field of materials science [19].

The gradient nanograined metals with a spatially graded variation of grain sizes from nanoscale in surface, to submicron, even micron in core, hereafter named as GNG/CG, are recently shown to possess a superior all-round fatigue resistance [24–27]. Previous study [27] focuses on the basic feature of fatigue properties of gradient nanograined Cu (GNG Cu), i.e. with superior combination of high-cycle fatigue limit and low-cycle fatigue life (at the strain amplitudes of 0.29% and 0.5%), compared to their homogeneous CG and UFG counterparts. Such an enhanced low-cycle fatigue resistance is attributed to an ordered strain accommodation and delocalization process with significant reduced dislocation density and homogeneous grain coarsening, as detected in fatigue tested GNG Cu at the strain amplitude of 0.5% [27]. In contrast, abnormal grain coarsening initiated from the subsurface layer, which postpones surface roughening and cracking and contributes to the enhanced high-cycle fatigue resistance, was reported in GNG Cu under stress control [28]. Besides, either abnormal or homogenous grain coarsening behaviors is detected in fatigue tested GNG Cu with different volume fractions of GNG layer under strain-controlled and stress controlled regimes [29, 30]. However, to date, the underlying mechanism dominating the abnormal or normal (homogeneous)

* Corresponding author.
*E-mail address:* llu@imr.ac.cn (L. Lu).

https://doi.org/10.1016/j.actamat.2020.06.047
1359-6454/

grain coarsening phenomenon in the gradient nanostructure under cyclic loading is still mystic yet.

In this work, to preclude the possible effect of the cyclic loading mode (i.e. stress and strain control) on the cyclic response, we designed a series of high-cycle and low-cycle fatigue tests of GNG/CG Cu samples under total strain amplitude control, covering a wide total strain amplitude spectrum from 0.12% to 0.55%. The fatigue properties (including cyclic response and fatigue life), microstructure and microhardness evolution in GNG layer of GNG samples in both high-cycle and low-cycle fatigue regimes are investigated, respectively. By comparing plastic strain amplitude and accumulative plastic strain profile in the GNG surface layer with different cycles, the underlying mechanisms determining the mode of grain coarsening and the size of coarsened grains are clarified.

## 2. Experimental

### 2.1. Sample preparation

Commercial-purity (99.98 wt%) Cu rods consisting of equiaxed coarse grains with an average grain size of 21 μm after being annealed at 450°C for 1 h are initially machined into dog-bone-shaped cylindrical samples with a gauge length of 12 mm and a gauge diameter of 6 mm. Then, their gauge sections are processed by the surface mechanical grinding treatment (SMGT) at cryogenic temperature (~173 K) with liquid nitrogen to produce a gradient nanograined (GNG) surface layer (i.e. GNG/CG Cu) [27, 31]. The detailed procedure for GNG sample preparation was described in detail in Ref. [27]. The as-processed GNG/CG Cu rod exhibits a smooth surface with a small surface roughness of ~300 nm and without detectable cracks.

### 2.2. Fully reversed tension-compression fatigue tests

Total strain controlled symmetric tension-compression fatigue tests of GNG/CG Cu and CG Cu samples with the same grain size of CG core in GNG sample are performed on an Instron 8874 testing machine at ambient temperature. A dynamic strain gauge extensometer with a gauge length of 10 mm and with a strain resolution better than 0.01% is applied to measure and to control the cyclic strain amplitude. A triangular waveform profile is applied with a cyclic strain rate of 0.2% $s^{-1}$ and a wide spectrum of total strain amplitude ($\Delta\varepsilon_t/2$) ranging from 0.12%, 0.2%, 0.3%, 0.5% and 0.55%, which spans mainly in the typical strain amplitude regime for single-crystal, CG and UFG Cu in strain-controlled low-cycle fatigue tests [5, 32-35]. Besides, a set of GNG/CG Cu specimens are cyclically deformed to different preset cycles (namely $N$ = 4%, 20% and 40%$N_f$) at $\Delta\varepsilon_t/2$ = 0.12% and 0.5% and then fully unloaded. To obtain each data set, at least three repeat cyclic loading tests of each case are performed at each $\Delta\varepsilon_t/2$.

### 2.3. Microstructural characterization

The cross-sectional microstructures of GNG/CG Cu after fatigue to failure are characterized via FEI Nova NanoSEM 430 field emission gun scanning electron microscope (SEM) with electron channel contrast imaging. Detailed microstructures of GNG/CG Cu fatigued to different cycles at $\Delta\varepsilon_t/2$ = 0.12% and 0.5% are also further investigated by FEI Tecnai F20 transmission electron microscope (TEM). To protect the GNG layer, a pure Cu layer is initially electro-deposited onto the treated surface of the GNG/CG samples. Then, the cross-sectional SEM and TEM foils are cut parallel to the cyclic loading axis by an electrical spark machine, and subsequently mechanically polished and electro-polished. The TEM Cu foils are finally thinned by twin-jet polishing in an electrolyte of phosphoric acid (25%), alcohol (25%) and deionized water (50%) at about −10 °C. Over 500 grains from numerous TEM images are measured to determine the average grain size in the 10 and 30 μm depths for GNG sample fatigued at different cycles.

### 2.4. Hardness tests

Microhardness tests are performed on the GNG/CG Cu samples in the as-SMGT state and those cyclically deformed to different cycles (namely $N$ = 4%, 20%, 40%$N_f$ and $N_f$) at $\Delta\varepsilon_t/2$ = 0.12%, 0.3% and 0.5% by a Mitutoyo MVK-H3 microhardness tester with a load of 5 g and a holding time of 10 s. The microhardness value at each depth of GNG/CG samples is obtained by averaging 10 measurements while the error bar is the mean ± standard deviation (SD).

## 3. Results

### 3.1. Strain controlled low-cycle and high-cycle fatigue properties of GNG/CG Cu

The as-processed GNG/CG Cu sample used in this study exhibits a spatially gradient microstructure, comprising NGs in the top 20 $\mu$m-thick layer, UFGs in a depth of 20 to 200 $\mu$m, deformed CG layer in the depth span of ~200–600 $\mu$m and then a deformation-free CG core. Both NG and UFG layers with a total thickness of 200 $\mu$m are hereafter referred to as the GNG layer. Most grains in the GNG layer contain a high density of dislocations and are separated by curved high-angle GBs, which are evidently in a high-energy non-equilibrium state, analogous to those in nanostructured metals and alloys produced by severe plastic deformation [9]. No strong crystallographic texture is detected in the GNG layer, as revealed via the electron backscatter diffraction measurement [27].

Both low-cycle and high-cycle fatigue tests of GNG/CG Cu and CG Cu samples are conducted under strain control, covering a wide $\Delta\varepsilon_t/2$ range, as shown in Fig. 1. Considered the fact that the "critical" $\Delta\varepsilon_t/2$ that divides low-cycle and high-cycle regimes of these GNG samples is approximately 0.29% [27], the GNG/CG Cu samples cyclically deformed at $\Delta\varepsilon_t/2$ of 0.12% and 0.2% belong to high-cycle fatigue regime while those at 0.3%, 0.5% and 0.55% are typical in low-cycle fatigue regime. At any given $\Delta\varepsilon_t/2$, GNG/CG Cu exhibits an elevated $\Delta\sigma/2$ level and longer fatigue life, relative to CG counterparts (Fig. 1a). Specially, at high-cycle small-amplitude regimes (i.e. $\Delta\varepsilon_t/2 < 0.29\%$), quasi cyclic stability with approximately constant stress amplitude ($\Delta\sigma/2$) is maintained in GNG/CG Cu after a short initially rapid hardening stage (~4%$N_f$). For example, the $\Delta\sigma/2$ of GNG/CG Cu fatigued at $\Delta\varepsilon_t/2$ of 0.12% rapidly increased to 106 MPa at ~4%$N_f$ and maintains nearly constant at about 106 MPa with a very small stress reduction (~2 MPa) in the subsequent cyclic deformation stage. A similar cyclic stability phenomenon is also detected for GNG/CG Cu cyclically deformed at low-cycle fatigue regimes ($\Delta\varepsilon_t/2 > 0.29\%$). Here, $\Delta\sigma/2$ of GNG/CG Cu fatigued at $\Delta\varepsilon_t/2$ of 0.5% quickly increases to 184 MPa at ~4%$N_f$ and maintains constant at ~184 MPa with a smaller stress variation (~0.4 MPa) till fatigue to failure.

The cyclic hardening rates of GNG/CG Cu at different $\Delta\varepsilon_t/2$, which is defined as the average stress increment per cycle, are plotted in Fig. 1b. For all $\Delta\varepsilon_t/2$ at both high-cycle and low-cycle fatigue regimes, GNG/CG samples exhibit a similar trend: cyclic hardening rate is high in the initial fatigue stage (~4%$N_f$), but dramatically reduces to a much smaller value (close to zero) in later fatigue stage, analogous to that of CG counterparts in Fig. 1b and reported in [32, 33, 36]. Specially, at any $\Delta\varepsilon_t/2$, the cyclic hardening rate of GNG/CG is smaller than that of CG counterpart at the same cycles. The quasi cyclic stability behavior of GNG/CG Cu with nearly constant stress amplitude and much smaller hardening rate in both low-cycle and high-cycle regimes is fundamentally distinct

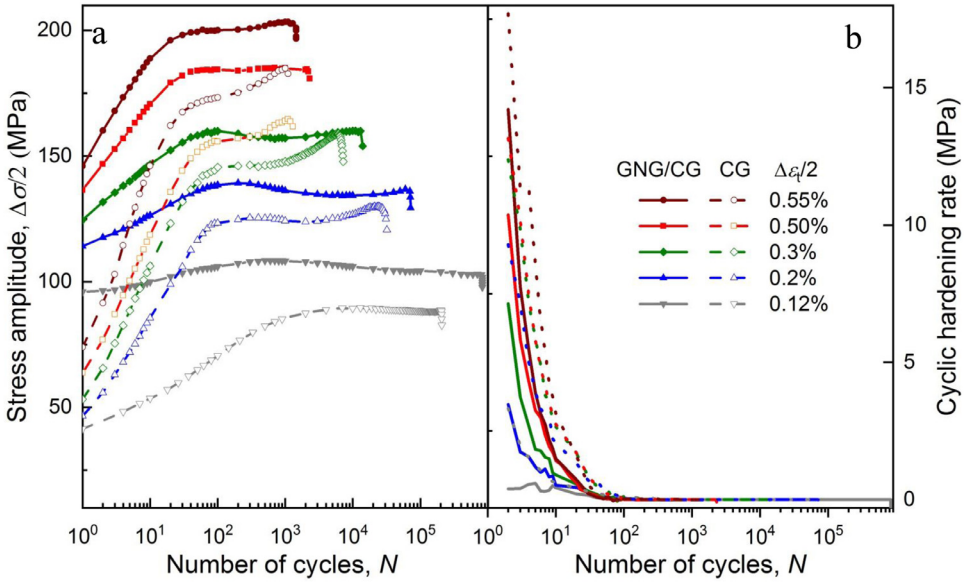


**Fig. 1.** Cyclic stress responses (a) and cyclic hardening rates (b) of GNG/CG Cu cyclically deformed at the total strain amplitudes ($\Delta\varepsilon_t/2$) ranging from 0.12% to 0.55%.

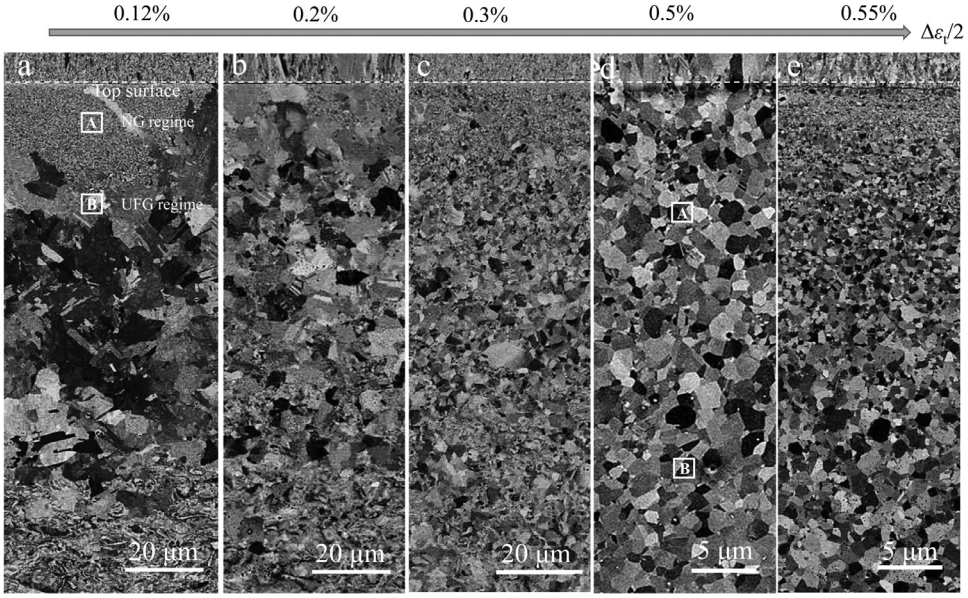


**Fig. 2.** Typical cross-sectional SEM images of surface GNG layer of GNG/CG Cu fatigued to failure at $\Delta\varepsilon_t/2$ of 0.12% (a), 0.2% (b), 0.3% (c), 0.5% (d), 0.55% (e), respectively. Dashed line represent the treated topmost surface. The evolution of NG and UFG structure in squares A and B inserted in (a) and (d) under cyclic loading are investigated via TEM, as shown in Figs. 3 and 4, respectively.

from the typical cyclic hardening of CG Cu [33, 37] and continuous cyclic softening of various nanostructured metals/alloys prepared by means of severe plastic deformation [5, 11, 19].

### *3.2. Cyclic deformation induced microstructural evolution in the GNG layer under different total strain amplitudes*

In order to exploit the effect of the imposed strain amplitudes on fatigue behavior of GNG surface layer on CG core, the cross-sectional microstructural evolutions of GNG/CG Cu cyclically deformed to failure at different $\Delta\varepsilon_t/2$ from 0.12% to 0.55% are systematically investigated by SEM, as shown in Fig. 2. Remarkably, grain coarsening generally occurs in the original gradient nanostructures of GNG/CG Cu during cyclic loading, but exhibiting different grain morphologies and grain sizes. For GNG/CG Cu cyclically deformed at small strain amplitude $\Delta\varepsilon_t/2 = 0.12\%$, as shown in Fig. 2a, abnormally large grains with an average size of 18.6 $\mu$m are prevalently detected in the whole subsurface UFG regions at a depth span of ~20–110 $\mu$m. However, only several large grains with a similar grain size are distributed locally in the topmost 20 $\mu$m-thick NG layer. Most of these coarse grains are in either elongated or in complex irregular shape and some twin boundaries can be found in these grain interiors. This indicates the occurrence of the abnormal grain coarsening in the GNG layer, the same as that observed in GNG/CG Cu under low-amplitude stress or strain control [28, 29].

With further increasing $\Delta\varepsilon_t/2$ to 0.3%, the abnormal large grains detected in Fig. 2a and b seldomly appear in the GNG layer (Fig. 2c). Instead, smaller coarsed grains are observed in the GNG layer, with a mean value of ~1.9 $\mu$m. Specially, less obvious coarsening is identified in NG layer, in contrast to the abnormal large grains detected in NG layer at $\Delta\varepsilon_t/2 = 0.12\%$ and 0.2%.

**Table 1**
Statistics of grain size in the original NG layer with a depth of 10 $\mu$m and UFG layer with a depth of 30 $\mu$m of GNG/CG Cu samples fatigued to failure at various $\Delta\varepsilon_t/2$.

| | AsSMGT | Cyclic deformation to failure at constant $\Delta\varepsilon_t$ /2 | | | | | |
|---|---|---|---|---|---|---|---|
| | | $\Delta\varepsilon_t$ /2 = | 0.12% | 0.2% | 0.3% | 0.5% | 0.55% |
| **Grain size at ~10 $\mu$m depth** | 75 ± 11 nm | Coarsed grain($\mu$m) | 18.6 ± 7.2 | 3.3 ± 1.6 | 1.8 ± 0.5 | 1.1 ± 0.2 | 0.5 ± 0.2 |
| | | Uncoarsed grain (nm) | 76 ± 23 | 80 ± 21 | 83 ± 19 | – | – |
| **Grain size at ~30 $\mu$m depth** | 205±64 nm | Coarsed grain ($\mu$m) | 16.8 ± 7.3 | 3.6 ± 1.0 | 1.9 ± 0.7 | 1.3 ± 0.5 | 0.6 ± 0.2 |
| | | Uncoarsed grain (nm) | 219 ± 75 | – | – | – | – |

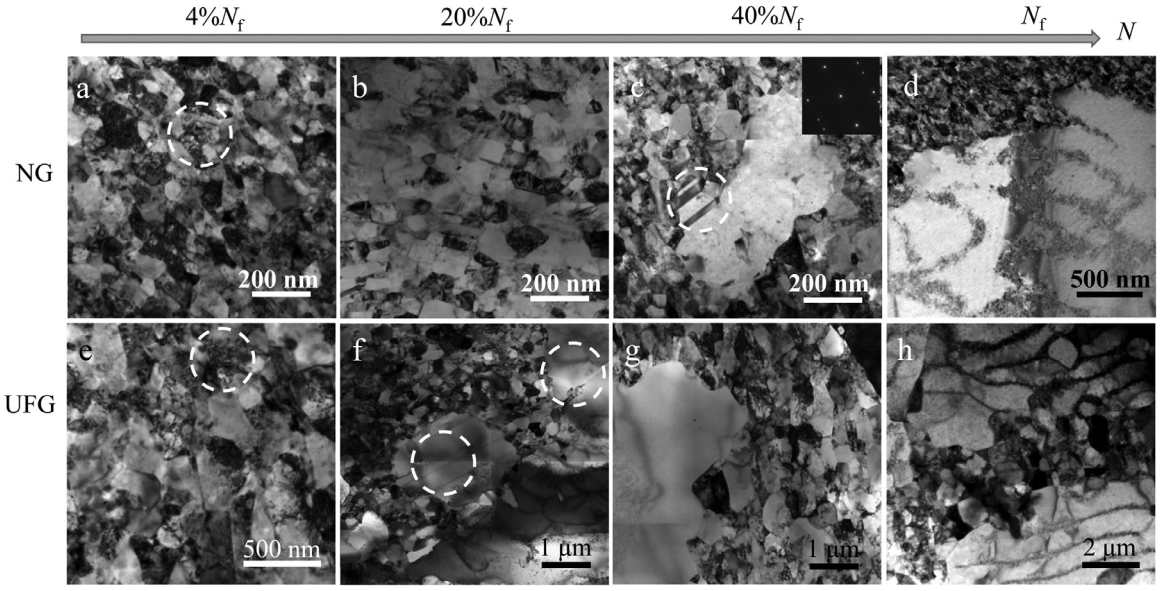


**Fig. 3.** Evolution of microstructure in the NG layer (~10 $\mu$m depth) (a–d) and UFG layer (~30 $\mu$m depth) (e–h) of GNG/CG Cu cyclically deformed at $\Delta\varepsilon_t/2$ of 0.12% at different number of cycles, as indicated. The inset in Fig. 3c is the corresponding selected area electron diffraction (SAED) patterns of twins in dashed circle.

Distinct from abnormal grain coarsening in the GNG layer at $\Delta\varepsilon_t/2$ smaller than 0.3% (Fig. 2a–b), relatively homogeneous grain coarsening, composed of roughly equiaxed micron-sized grains, is detected in the GNG layer cyclically deformed at $\Delta\varepsilon_t/2$ of 0.5% and 0.55% (Fig. 2d and e). These grains at $\Delta\varepsilon_t/2$ of 0.5% are in a much smaller size (~1 $\mu$m), relative to those at lower $\Delta\varepsilon_t/2$ and become finer at larger $\Delta\varepsilon_t/2$ of 0.55%. Interestingly, no macroscopic shear band is detected in the GNG layer at any $\Delta\varepsilon_t/2$ in Fig. 2. The measured grain size in the original NG layer with a depth of 10 $\mu$m and UFG layer with a depth of 30 $\mu$m of GNG/CG Cu samples fatigued to failure at various $\Delta\varepsilon_t/2$ are summarized in Table 1.

To understand the microstructural evolutions of abnormal and normal grain coarsening behaviors during cyclic deformation, both the UFG and NG regimes (marked by the white squares in Fig. 2a and d) of GNG/CG Cu fatigued at $\Delta\varepsilon_t/2$ of 0.12% and 0.5% with different cycles were further studied by TEM observations. After 33,000 cycles at $\Delta\varepsilon_t/2$ of 0.12%, about 4%$N_f$ the microstructure in the GNG layer (Fig. 3a and e) is still kept stable as that in the as-SMGTed state [27]. The NGs and UFGs are still separated by curved GBs with a high density of dislocations (highlighted by dashed cycle in Fig. 3a and b) and with mean grain sizes of 76 and 219 nm, comparable to that of as-SMGTed sample (Table 1). After 20%$N_f$, no obvious change either in grain morphology or in grain size is observed in surface NG layer, except slightly microstructural recovery with reduced dislocation density in grain interiors or at GBs (Fig. 3b).

In contrast, a few abnormally large grains containing a relatively low density of dislocations have occurred in the subsurface UFG layer (Fig. 3f). Until 40%$N_f$, sporadic large grains can be also detected in the 10 μm-deep NG matrix (Fig. 3c), like that observed in the subsurface UFG layer in Fig. 3f and g. We notice that some twin boundaries in micron width (highlighted by dashed cycle) exist in some larger grains, which can be verified by the selected-area electron diffraction (SAED) patterns inserted in Fig. 3c, consistent with that shown in Fig. 2a. With further increasing cycles before failure, abnormal grains become coarser and coarser, via consuming the surrounding UFG and NG grains (Fig. 3d and h). Typical dislocation patterns, dislocation walls or cells, are also identified in these coarse grains, just like that in fatigue tested monocrystal and CG Cu [32, 38–40]. Even after 8.2 × $10^5$ cycles ($N_f$), numerous UFGs and NGs are still remnant in the GNG layer.

Differently, TEM observations shown in Fig. 4 indicate continuous, homogeneous grain coarsening in NG and UFG layers at $\Delta\varepsilon_t/2$ = 0.5%. After 100 cycles, 4%$N_f$, both NG and UFG layer have suffered from detectable microstructure changes, with a strikingly reduced intra-crystalline dislocation density and increased grain size (Fig. 4a and e). The average grain size of the NG and UFG layer at 4%$N_f$ is increased to ~117 nm and ~ 245 nm, respectively, both are larger than that before fatigue tests (~75 and 205 nm). With further increasing cycles, grains become larger, separated by sharp GBs, with few dislocations in grain interiors (Fig. 4b and c and 4f and g). Twin boundaries can also be detected in some coarse grains, as highlighted by dashed cycle (Fig. 4b and d), analogous to that in Fig. 3c and f at $\Delta\varepsilon_t/2$ = 0.12%. Eventually, after repeated loading over ~2600 cycle until failure, homogeneous equiaxed micron sized grains containing few dislocations with distinct GBs are

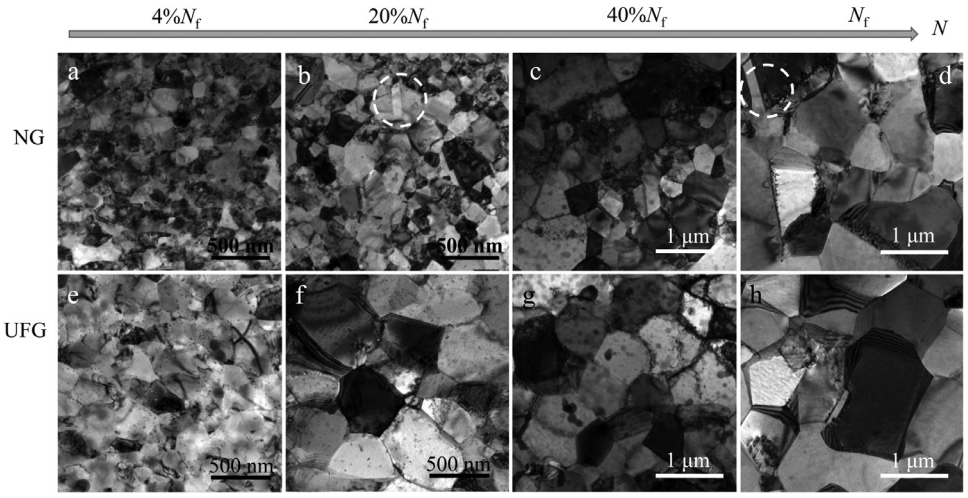


**Fig. 4.** Evolution of microstructure in the NG layer (~10 $\mu$m depth) (a-d) and UFG layer (~30 $\mu$m depth) (e-h) of GNG/CG Cu cyclically deformed at $\Delta\varepsilon_t/2 = 0.5\%$ at different number of cycles, as indicated.

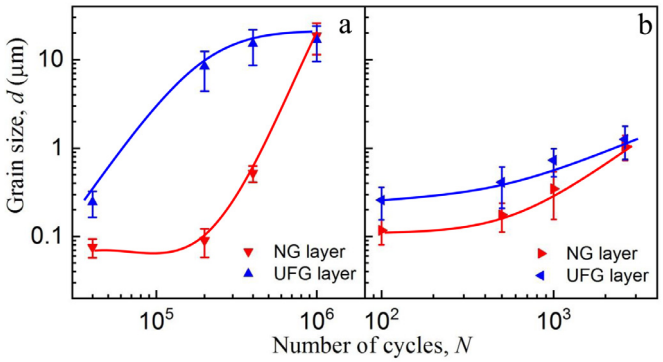


**Fig. 5.** Measured grain size versus number of cycles for the original NG layer with a depth of 10 μm and UFG layer with a depth of 30 μm of GNG/CG Cu fatigued at $\Delta\varepsilon_t/2 = 0.12\%$ (a) and 0.5% (b).

detected in the GNG layer (Fig. 4d and h), the same as that reported in [27]. Only a few dislocation tangles or dislocation debris are occasionally found at some GBs or in several grain interiors, which is different from that in abnormal coarsed grains at low $\Delta\varepsilon_t/2$ (Fig. 3).

## 4. Discussion

### *4.1. Homogeneous and abnormal grain coarsening in the gradient nanostructure*

Fig. 5a and b showed the grain size variation in NG and UFG layers cyclically deformed as a function of number of cycles at $\Delta\varepsilon_t/2$ of 0.12% and 0.5%, respectively. Irrespective of abnormal or homogeneous grain coarsening modes, the grains that coarsen in the GNG layer become larger monotonically with increasing number of cycles. In particular, both the NG and UFG layers have comparable final coarsed grains in size after fatigue failure at both $\Delta\varepsilon_t/2$ (Fig. 5, Table 1), although the initial mean grain size of NGs is much smaller than that of UFGs. Besides, the comparison of Fig. 5a and b clearly shows that the final abnormal coarsed grain size (~16.8–18.6 $\mu$m) in the GNG layer at $\Delta\varepsilon_t/2 = 0.12\%$ is much larger than that of homogeneous coarsed grains (~1 $\mu$m) at $\Delta\varepsilon_t/2 = 0.5\%$.

In order to further explore the mechanical characteristic of abnormal and homogeneous grain coarsening behavior, we perform

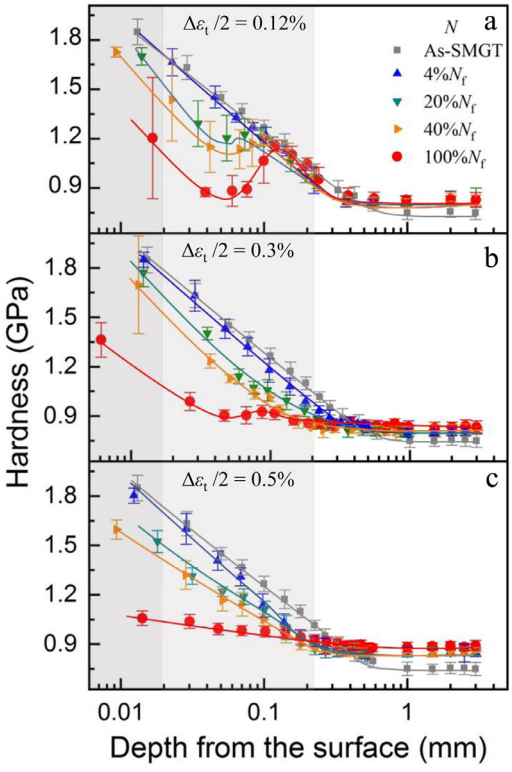


**Fig. 6.** Variations of microhardness with the number of cycles along the depth from the surface of GNG/CG Cu fatigued at $\Delta\varepsilon_t/2$ of 0.12% (a), 0.3% (b) and 0.5% (c) respectively. The areas with the gray, light gray and white background in a, b and c indicates the top NG layer, UFG layer, deformed CG layer and CG core, respectively.

microhardness (*Hv*) tests on GNG/CG Cu samples before fatigue and those cyclically loaded at $\Delta\varepsilon_t/2 = 0.12\%$, 0.3% and 0.5% with different cycles (namely $N$ = 4%, 20%, 40%$N_f$ and $N_f$), as shown in Fig. 6a–c, respectively. For the sample in the as-SMGTed state, the microhardness is gradiently distributed from the top surface (*Hv* =1.85 GPa) to the CG core (*Hv* = 0.75 GPa). With increasing cyclic number, cyclic hardening occurs in the CG core (white background region) while cyclic softening in the NG (gray background region) and UFG layer (light gray background region), but exhibiting different *Hv* profiles at different $\Delta\varepsilon_t/2$.

At $\Delta\varepsilon_t/2 = 0.12\%$, the *Hv* profile in the NG layer and UFG layer fatigue tested in initial cycles ($N < 4\%\ N_f$) nearly overlaps with that of as-SMGTed state (Fig. 6a). Untill at 20% $N_f$, a noteworthy drop of hardness with a value of 1.20 ± 0.14 GPa (forming a small *Hv* valley) is detected at ~ 50 $\mu$m depth beneath the surface with an initial grain size of ~200 nm. With further increasing cycles, the *Hv* valley gradually extends to the top surface and to the deeper interior with a continuously reduced hardness simultaneously. Eventually, at $N_f$, a large valley spans from topmost NG surface to ~100 $\mu$m depth. In particular, the average hardness in the topmost surface decreases to ~1.23 GPa with a very large standard deviation of ±0.37 GPa.

With increasing $\Delta\varepsilon_t/2$ to 0.3% and 0.5% (Fig. 6b and c), the *Hv* profiles in GNG layer with increasing cycles are distinct from that at $\Delta\varepsilon_t/2 = 0.12\%$ (Fig. 6a). In initial cycles ($N < 4\%\ N_f$), *Hv* drops slightly in the NG layer and a rapid *Hv* reduction is found in the subsurface UFG layer, especially at a larger $\Delta\varepsilon_t/2$ of 0.5%. With increasing the number of cycles, an obvious monotonic drop of hardness occurs in the whole GNG layer (Fig. 6b and c). The *Hv* at topmost surface of GNG/CG Cu at $N_f$ has declined to 1.1 ± 0.04 GPa, slightly higher than that in the subsurface UFG layer (i.e. 0.94±0.04 GPa at 200 $\mu$m depth) and CG core (0.89±0.03 GPa), indicating that the *Hv* gradient between GNG layer and CG core in the as-SMGT GNG sample disappears after fatigue.

### 4.2. Distribution of plastic strain effect on grain coarsening mode

The observed different evolution trends of *Hv* profiles at different $\Delta\varepsilon_t/2$ in Fig. 6 suggest that the cyclic deformation mechanism, i.e. the mode of grain coarsening modes during cyclic loading, should be closely correlated with the cyclic plastic straining in the GNG layer. Under the constant $\Delta\varepsilon_t/2$, it's reasonably assumed that the sum of elastic strain amplitude ($\Delta\varepsilon_e/2$) and plastic strain amplitude ($\Delta\varepsilon_{pl}/2$) is maintained constant for different layers of the gradient nanostructure during cyclic loading:

$$\Delta\varepsilon_t/2 = \Delta\varepsilon_e/2 + \Delta\varepsilon_{pl}/2 = \Delta\sigma/2E + \Delta\varepsilon_{pl}/2 \quad (1)$$

Where $\Delta\sigma/2$ is the stress amplitude and $E$ is the Young's modulus (120 GPa for Cu).

According to the estimate of $\Delta\sigma/2$ by using *Hv* spatially distributed in the GNG layer and stress amplitude data of GNG/CG and CG in Fig. 1 (see the detail in Appendix A. Suppementary data), the plastic strain amplitude ($\Delta\varepsilon_{pl}/2$) contours in the GNG layer with different number of cycles at $\Delta\varepsilon_t/2 = 0.12\%$ and 0.5% are calculated and plotted in Fig. 7. For GNG/CG Cu cycled at $\Delta\varepsilon_t/2 = 0.12\%$ at $N < 4\%N_f$ (Fig. 7a), the overall GNG surface layer mainly deforms elastically, owing to the presence of high strength NGs and UFGs. At 20%$N_f$, plastic deformation with $\Delta\varepsilon_{pl}/2$ larger than 0.01% concentrates locally in the subsurface layer with a depth of about 50 $\mu$m (Fig. 7b). With increasing cycles, more and more isolated plastic deformation regions are localized in the subsurface UFG layer. At $N_f$, the GNG layer within 100 μm depth exhibits a $\Delta\varepsilon_{pl}/2$ of ~0.02%, which is also comparable to that of free-standing CG counterpart at the same fatigue condition. Note that the UFG layer with larger grain size and/or dislocation structure at the ~150–200 μm depth undergoes somewhat plastic strain, mainly as a consequence of high density dislocation activity such as dislocation recovery and annihilation (Fig. 7a–d).

By contrast, the $\Delta\varepsilon_{pl}/2$ contours in GNG/CG Cu fatigue tested at $\Delta\varepsilon_t/2 = 0.5\%$, as shown in Fig. 7e–h, is fully distinct from the case at $\Delta\varepsilon_t/2 = 0.12\%$ (Fig. 7a–d). Even at initial 4%$N_f$, plastic deformation has occurred in the whole subsurface UFG layer (Fig. 7e). In particular, the plastic strain amplitude is gradiently distributed in the subsurface UFG layer, with $\Delta\varepsilon_{pl}/2$ decreasing from ~0.3% in ~200 μm depth to ~0.1% at ~20 μm depth, an order of magnitude higher than that of GNG sample at $\Delta\varepsilon_t/2 = 0.12\%$ at the same depth (Fig. 7a). With increasing cycles, the cyclic plastic strain with larger $\Delta\varepsilon_{pl}/2$ progressively moves to the neighboring top NG layer (Fig. 7f and g). At $N_f$, plastic strain with a $\Delta\varepsilon_{pl}/2$ of ~0.3% is almost homogeneously distributed in the whole GNG surface layer (Fig. 7h).

Obviously, the gradient nanostructure exhibits different $\Delta\varepsilon_{pl}/2$ profiles when cyclically deformed at different $\Delta\varepsilon_t/2$. At small $\Delta\varepsilon_t/2$ (i.e. 0.12%), most grains in the GNG layer deformed elastically (Fig. 7b and c), and plastic strain occurs only in sporadically and randomly distributed sites of the subsurface UFG layer with relatively soft orientation or larger grain size [28]. With increasing cycles, the local distributed $\Delta\varepsilon_{pl}/2$ thus activates the abnormal grain coarsening with decreased defects and the correlated softening, which further promotes or accelerates the plastic straining. Hence, the cyclic plastic strain more readily concentrates these, but can not homogeneously transforms in the whole GNG layer.

In contrast, when imposed a larger strain amplitude (such as 0.5%), almost all UFGs within a certain depth layer is in the state of plastic deformation and with gradient distributed $\Delta\varepsilon_{pl}/2$ (Fig. 7e–g). As a result, mechanical driven grain boundary migration occurs there, which naturally stimulates the adjacent layer with finer grains to accommodate plastic strain, analogous to the case that the stress concentration produced by a dislocation pileup in one grain can activate dislocation sources and plastic deformation in the adjacent grain during tensile tests [41]. Cyclic plastic strain with a large $\Delta\varepsilon_{pl}/2$ will progressively propagate to the whole GNG layer (Fig 7f and g), and such delocalized strain feature enables the occurrence of homogeneous coarsening. It has to be noted here that the critical $\Delta\varepsilon_t/2$ is 0.29% because it is approximately the maximum elastic straining of most UFGs with a hardness of 1.0–1.2 GPa.

The forgoing analysis demonstrates that the grain coarsening mode in either abnormal or normal mode is mainly determined by the spatial distribution and propagation features of the cyclic plastic strain (localized or delocalized) under cyclic loading. Such a unique fatigue behavior of GNG metal is fundamentally different from the randomly distributed strain-localized fatigue behavior of nanostructured metals prepared via severe plastic deformation [10, 14–16, 20]. The presence of ductile CG core also benefits for suppressing macroscopic strain localized behavior (such as shear banding) and triggering the change of grain coarsening mode in the GNG layer.

### 4.3. Locally cumulative plastic strain effect on coarsened grain size

Results from Figs. 2–5 also show that the final coarsed grain size in the GNG layer becomes larger when cycled at smaller total strain amplitude. Evidently, the degree of grain coarsening in the GNG layer during cyclic deformation is not positively correlated with the imposed large total strain amplitude or cyclic stress amplitude. Since the grain coarsening in both modes is a consequence of cyclic plastic straining, thus, its degree should be determined by another important fatigue parameter, i.e. cumulative plastic strain ($\Sigma 4\Delta\varepsilon_{pl}/2$) [32].

The $\Sigma 4\Delta\varepsilon_{pl}/2$ contours in the GNG layer at different number of cycles can be roughly estimated by summing up the measured plastic strain amplitude of GNG/CG Cu during cyclic loading (See details in Ref. [27]). Again, taking GNG/CG Cu sample fatigued at $\Delta\varepsilon_t/2 = 0.12\%$ and 0.5% as typical examples, the $\Sigma 4\Delta\varepsilon_{pl}/2$ in the GNG layer monotonically increases with increasing number of fatigue cycles, as shown in Fig. 8. Specially, for GNG/CG Cu at $\Delta\varepsilon_t/2$ of 0.12%, the estimated $\Sigma 4\Delta\varepsilon_{pl}/2$ in isolated island-like regions at the 50-μm-deep subsurface layer is very large, about 40 at 20%$N_f$ (Fig. 8b). At $N_f$, most GNG layer sustains a total accumulated plas-

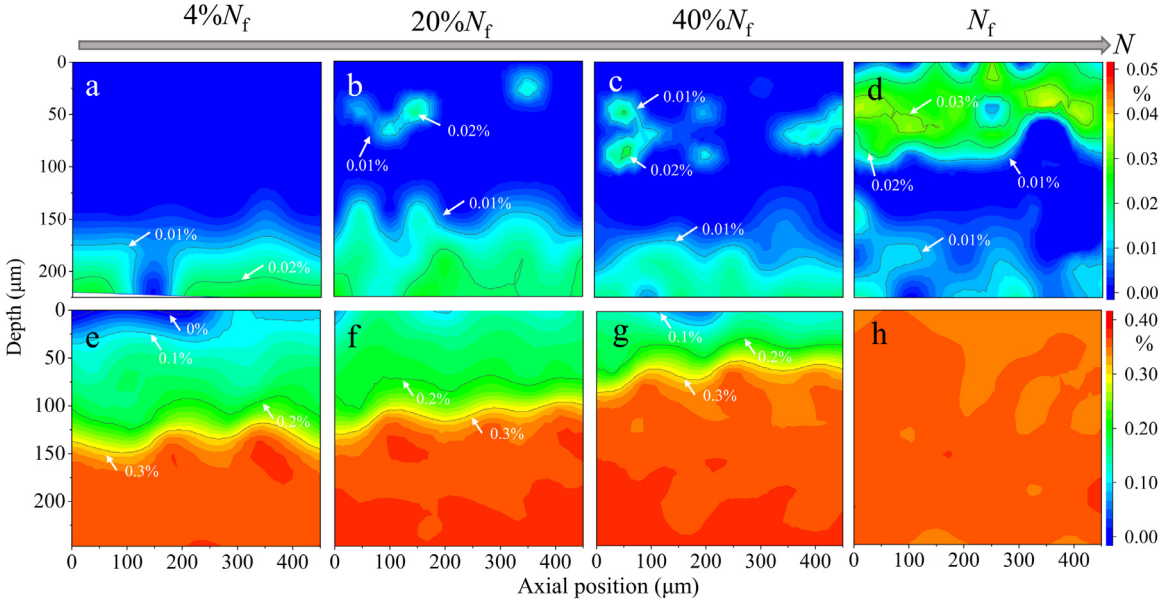


**Fig. 7.** Plastic strain amplitude ($\Delta\varepsilon_{pl}/2$) contour in the GNG layer of GNG/CG Cu fatigued to different number of cycles at $\Delta\varepsilon_t/2$ of 0.12% (a–d) and 0.5% (e–h): $N = 4\%N_f$ (a, e), $20\%N_f$ (b, f), $40\%N_f$ (c, g), and $100\%N_f$ (d, h).The contour lines in (a–g) denote the critical regions with the same plastic strain amplitude ($\Delta\varepsilon_{pl}/2$), measured by the color bar on the right. The $\Delta\varepsilon_{pl}/2$ of some contour lines are labelled.

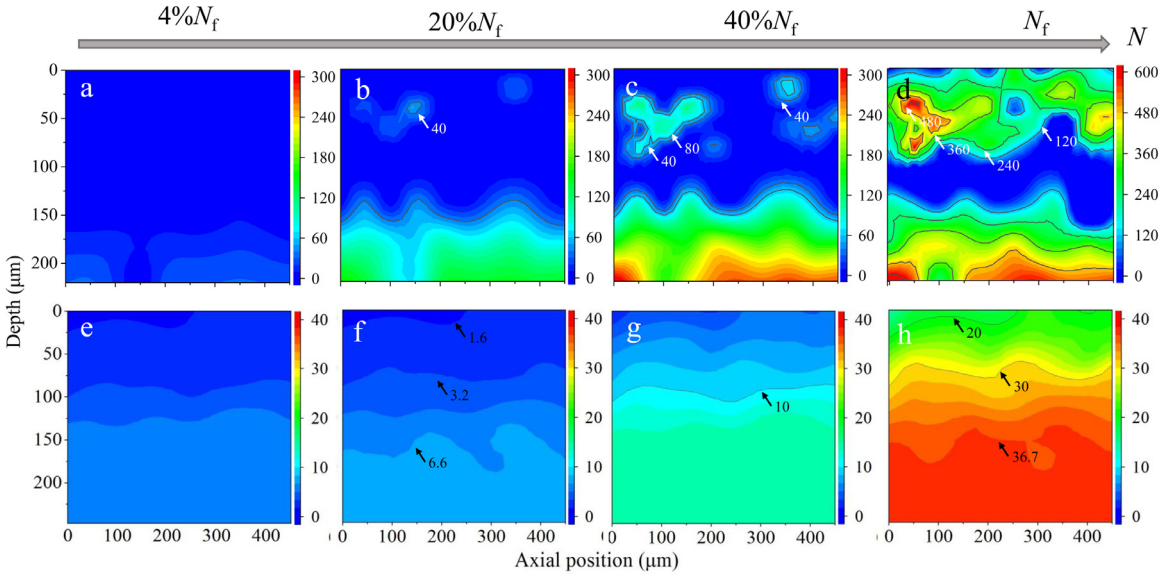


**Fig. 8.** Cumulative plastic strain ($\Sigma 4\Delta\varepsilon_{pl}/2$) contour in the GNG layer of GNG/CG Cu fatigued to different number of cycles at $\Delta\varepsilon_t$ /2 of 0.12% (a-d) and 0.5% (e-h): $N = 4\%N_f$ (a, e), $20\%N_f$ (b, f), $40\%N_f$ (c, g), and $100\%N_f$ (d, h). The contour lines in (a-g) denote the critical regions with the same $\Sigma 4\Delta\varepsilon_{pl}/2$, measured by the color bar on the right.

tic strain of larger than 300, at some local regions as large as ~420 (Fig. 8d).

Differently, the $\Sigma 4\Delta\varepsilon_{pl}/2$ is gradiently distributed in the GNG layer of GNG/CG Cu cycled at $\Delta\varepsilon_t/2 = 0.5\%$ during the whole fatigue stage, as shown in Fig. 8e–h. At $20\%N_f$, $\Sigma 4\Delta\varepsilon_{pl}/2$ at topmost NG surface is ~1.6 and it gradually increases to ~6.6 at subsurface UFG layer at depth of ~220 $\mu$m (Fig. 8f). At $N_f$, $\Sigma 4\Delta\varepsilon_{pl}/2$ in both NG and UFG layer has increased up to ~20 and 36.7 (Fig. 8h), much larger than that accommodated in CG Cu (~20) [27, 32], but more than an order of magnitude smaller than that cyclically deformed at $\Delta\varepsilon_t/2 = 0.12\%$ (Fig. 8d).

The average grain sizes versus cumulative plastic strain in the 10 μm-depth NG layer and 30 μm-depth UFG layer of GNG/CG Cu fatigued at $\Delta\varepsilon_t$ /2 = 0.12% and 0.5% are plotted in Fig. 9. The grain size of NG layer in tensile tested GNG/CG Cu [31, 42] are also included in Fig. 9 where the grain size increases with increasing the tensile strain. Analogous to the grain size coarsening trend in tensile test, the coarsed grain size in the NG and UFG layers of cyclically deformed GNG/CG Cu at $\Delta\varepsilon_t$ /2 = 0.12% and 0.5% monotonically increases with $\Sigma 4\Delta\varepsilon_{pl}/2$. Specially, as highlighted by dotted cycle in Fig. 9, the coarsed size (~620 nm) in the NG layer at $\Delta\varepsilon_t/2 = 0.12\%$ is approximately comparable to that (~700 nm) of UFGs at $\Delta\varepsilon_t$ /2 = 0.5%, although at different strain amplitudes and fatigue cycles, but this case can be achieved solely because they undergo a comparable $\Sigma 4\Delta\varepsilon_{pl}/2$. High density of non-equilibrium UFGs and NGs with high stored energy in the GNG layer itself benefit for GB migration and grain coarsening, but which is not the key factor of controlling the grain coarsening behavior of GNG sample with the same microstructure and stored GB energy fatigue tested at different $\Delta\varepsilon_t/2$. Thus, it can be concluded that the size of

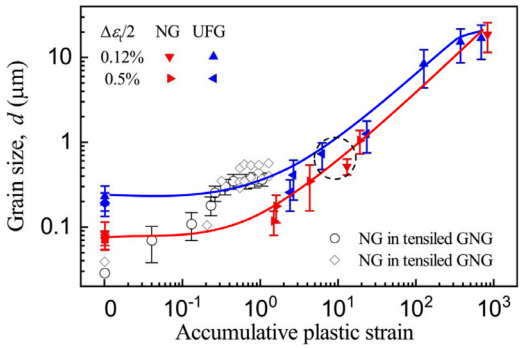


**Fig. 9.** Grain size versus accumulative plastic strain of GNG/CG Cu fatigued at different cycles at $\Delta\varepsilon_t/2$ = 0.12% and 0.5% (c).The variation of average grain size of NG layer in GNG Cu as a function of tensile strains reported in [31, 42] are also included for comparison.

abnormal or normal coarsed grain with increasing cycles is predominantly dependent on the accumulated plastic strain, instead of the imposed total/plastic strain amplitude or stress amplitude or number of cycles or stored GB energy. After undergoing a larger cumulative plastic strain, the GNG layer at small $\Delta\varepsilon_t/2$ thus exhibits a larger abnormal coarsed grain size than that of homogeneous coarsened grains at larger $\Delta\varepsilon_t/2$. That's also the reason why the final coarsed grain size is much larger than the case of GNG/CG Cu in tensile tests (~400 nm) [31, 42]. We would like to emphasize here that the influence of purity and the processing-induced contaminations (such as carbon, oxygen, and nitrogen) in the surface layer of GNG Cu on the mode and extent of grain coarseningin are negligible in view of the high-purity of raw Cu rods (99.98 wt.%) and much smaller contaminated depth ($< 0.5\ \mu$m) [43].

Cyclic hardening of GNG mainly occurs in the early stage of fatigue life (i.e. $N < 4\%N_f$), as shown in Fig. 1b. The higher cyclic hardening rate detected in GNG/CG Cu at larger $\Delta\varepsilon_t/2$ is mainly dominated by the enhanced cyclic hardening of CG core, instead of the grain coarsening which does not occur obviously in GNG layer at the initial fatigue period. This is because the overall cyclic responses of GNG/CG are the coupled effect of cyclic behaviors of GNG surface layer and CG core. As shown in Figs. 1 and 6, obvious cyclic hardening with a higher hardening rate at larger $\Delta\varepsilon_t/2$ is detected in the CG core (approximately comparable to the free-standing CG) when $N < 4\%N_f$, due to the generation and accumulations of higher density of forest dislocations in CG core [32, 33]. But there are almost no changes in microhardness of GNG surface layer at small $\Delta\varepsilon_t/2$ (i.e. 0.12%) and slightly softening at larger $\Delta\varepsilon_t/2$ (i.e. 0.5%), without obvious grain coarsening yet at this fatigue period, as shown in Figs. 3–6.

With increasing cycles ($N > 4\%N_f$), cyclic straining induces either abnormal grain coarsening at small $\Delta\varepsilon_t/2$ or normal grain coarsening at large $\Delta\varepsilon_t/2$, thus rapidly softening occurs in the partial or the whole GNG layer, as shown in Fig. 6. This, together with the less pronounced cyclic hardening in CG core especially at smaller $\Delta\varepsilon_t/2$, results in a rapidly reduced cyclic hardening of the whole GNG sample with almost zero hardening rate and cyclic stability under strain control (Fig. 1).

For GNG/CG Cu at low stress amplitude or $\Delta\varepsilon_t/2$, previous studies has showed that only after the abnormal micron sized grains has reached the topmost surface of fatigued GNG/CG Cu, surface micron-scale extrusions and cracking can be formed in the surface [28, 29], analogous to that occurred in fatigue tested CG metals [34, 40, 44–46]. Differently, the fluctuations in surface asperities of GNG/CG Cu cyclically deformed at larger $\Delta\varepsilon_t/2$, such as 0.5%, is obviously reduced and much smaller than that at smaller $\Delta\varepsilon_t/2$ [27]. This mainly arises from de-localized progressive strain transmission associated with homogeneous grain coarsening and the relatively small coarsened grain size in the surface GNG (Fig. 2d and Fig.7e–h), compared to the characteristic dimension of dislocation structures (~1 μm) [32, 40].

Overall, either abnormal grain coarsening or homogeneous grain coarsening in the GNG layer can essentially retard or suppress surface roughening and fatigue cracking, contributing to an enhancement of both high-cycle and low-cycle fatigue lives of GNG/CG Cu. The findings of this study demonstrate that although the GB migration and grain coarsening induced softening of nanostructured metals during mechanical stimuli, the unique grain coarsening behavior in gradient nanostructure can effectively accommodate cyclic plastic strain and benefit for enhancing fatigue life of gradient nanostructured metals.

## 5. Conclusion

Through designing a series of high-cycle and low-cycle fatigue tests with a wide total strain amplitude range from 0.12% to 0.55%, we show, for the first time, that the transition from abnormal to normal (or homogeneous) coarsening in GNG Cu with increasing strain amplitude is mainly determined by the spatial distribution of the plastic strain and its non-localized propagation in the GNG layer. Moreover, the final size of coarsened grains in both modes primarily depend on the cumulative plastic strain, instead of imposed stress/strain amplitude, number of cycles and total GB energy stored in the GNG layer. These findings deepen our understanding of cyclic behavior of gradient nanostructured metal and may provide insights on tailor-designing fatigue-resistant engineering structures.

## Acknowledgments

The authors acknowledge financial support by National Science Foundation of China (NSFC, Grant Numbers. U1608257 and 51931010), the Key Research Program of Frontier Science and International partnership program (Grant Number. GJHZ2029), CAS, and LiaoNing Revitalization Talents Program (Grant Number. XLYC1802026). Q.P. acknowledges support by NSFC (Grant Number. 51601196) and Youth Innovation Promotion Association CAS (Grant Number. 2019196).

## Appendix A. Calculation of plastic strain amplitude in the GNG layer

For the nano or ultrafine grains in the GNG layer (with slightly coarsening and limited strain hardening capacity) at the initial fatigue stage (namely $N = 4\%, 20\%N_f$), their stress amplitude ($\Delta\sigma/2$) or yield strength are estimated to be approximately one third of the measured *Hv* (which should be much closer to ultimate tensile strength, $\sigma_{UTS}$) .

With further cycling, obvious grain coarsening either in normal or abnormal mode occurs the gradient nanostructure, and its strain hardening capacity as well as the difference between $\sigma_y$ and $\sigma_{UTS}$ increase in larger grain size, indicating that their $\Delta\sigma/2$ is not accurately estimated using the *Hv* data. In view of this, we therefore utilized the other method to estimate the $\Delta\sigma/2$ in GNG layer with larger grain size and at longer fatigue cycles ($N = 40\%, N_f$), based on the reasonable hypothesis that the ratio of $\Delta\sigma/2$ in different depth of the GNG layer to that in CG core is approximately proportional to the ratio between their hardness.

According to the Eq. (1) in the manuscript, in combination of the estimated $\Delta\sigma/2$ by using *Hv* spatially distributed in the GNG layer and stress amplitude data of GNG/CG and CG in Fig. 1, the plastic strain amplitude ($\Delta\varepsilon_{pl}/2$) contours in the GNG layer with

different number of cycles at $\Delta\varepsilon_t/2 = 0.12\%$ and 0.5% are calculated and plotted in Fig. 7. The estimated $\Delta\varepsilon_{pl}/2$ in GNG layer at $N_f$ is comparable to that in the CG counterpart, calculated from the hysteresis loop, suggesting that the estimations of $\Delta\varepsilon_{pl}/2$ in this study are rational and reliable, even though it is relatively rough.

## References


[1] H. Gleiter, Nanocrystalline materials, Prog. Mater. Sci. 33 (1989) 223–315.
[2] J. Chen, L. Lu, K. Lu, Hardness and strain rate sensitivity of nanocrystalline Cu, Scr. Mater. 54 (2006) 1913–1918.
[3] K. Lu, Stabilizing nanostructures in metals using grain and twin boundary architectures, Nat. Rev. Mater. 1 (2016) 16019.
[4] S.R. Agnew, A.Y. Vinogradov, S. Hashimoto, J.R. Weertman, Overview of fatigue performance of Cu processed by severe plastic deformation, J. Electron. Mater. 28 (1999) 1038–1044.
[5] H. Mughrabi, H.W. Höppel, Cyclic deformation and fatigue properties of very fine-grained metals and alloys, Int. J. Fatigue 32 (2010) 1413–1427.
[6] Q.S. Pan, L. Lu, Strain-controlled cyclic stability and properties of Cu with highly oriented nanoscale twins, Acta Mater. 81 (2014) 248–257.
[7] T. Hanlon, Y.N. Kwon, S. Suresh, Grain size effects on the fatigue response of nanocrystalline metals, Scr. Mater. 49 (2003) 675–680.
[8] H. Mughrabi, H.W. Höppel, M. Kautz, Fatigue and microstructure of ultrafine–grained metals produced by severe plastic deformation, Scr. Mater. 51 (2004) 807–812.
[9] M.A. Meyers, A. Mishra, D.J. Benson, Mechanical properties of nanocrystalline materials, Prog. Mater. Sci. 51 (2006) 427–556.
[10] A. Vinogradov, S. Hashimoto, Multiscale phenomena in fatigue of ultra-fine grain materials – an overview, Mater. Trans. JIM 42 (2001) 74–84.
[11] H.W. Höppel, M. Brunnbauer, H. Mughrabi, Cyclic deformation behaviour of utrafine-grained size copper produced by equal channel angular pressing, in: Werkstoffwoche Partnerschaft (Ed.), Proceedings of Materials Week 2000, Frankfurt, German, 2000, pp. 1–8.
[12] Z.J. Zhang, X.H. An, P. Zhang, M.X. Yang, G. Yang, S.D. Wu, Z.F. Zhang, Effects of dislocation slip mode on high-cycle fatigue behaviors of ultrafine-grained Cu-Zn alloy processed by equal-channel angular pressing, Scr. Mater. 68 (2013) 389–392.
[13] X.H. An, S.D. Wu, Z.G. Wang, Z.F. Zhang, Enhanced cyclic deformation responses of ultrafine-grained Cu and nanocrystalline Cu–Al alloys, Acta Mater. 74 (2014) 200–214.
[14] S.D. Wu, Z.G. Wang, C.B. Jiang, G.Y. Li, I.V. Alexandrov, R.Z. Valiev, The formation of PSB-like shear bands in cyclically deformed ultrafine grained copper processed by ECAP, Scr. Mater. 48 (2003) 1605–1609.
[15] M. Goto, S.Z. Han, T. Yakushiji, C.Y. Lim, Kim, Formation process of shear bands and protrusions in ultrafine grained copper under cyclic stresses, Scr. Mater. 54 (2006) 2101–2106.
[16] P. Lukáš, L. Kunz, M. Svoboda, Fatigue mechanisms in ultrafine-grained copper, Kovove Mater. 47 (2009) 1–9.
[17] B.L. Boyce, H.A. Padilla, Anomalous fatigue behavior and fatigue-induced grain growth in nanocrystalline nickel alloys, Metall. Mater. Trans. A 42A (2011) 1793–1804.
[18] C.C.F. Kwan, Z. Wang, Strain incompatibility and its influence on grain coarsening during cyclic deformation of ARB copper, Philos. Mag. 93 (2012) 1065–1079.
[19] A. Pineau, A. Amine Benzerga, T. Pardoen, Failure of metals III: fracture and fatigue of nanostructured metallic materials, Acta Mater. 107 (2016) 508–544.
[20] T.A. Furnish, A. Mehta, D. Van Campen, D.C. Bufford, K. Hattar, B.L. Boyce, The onset and evolution of fatigue-induced abnormal grain growth in nanocrystalline Ni-Fe, J. Mater. Sci. 52 (2017) 46–59.
[21] L. Kunz, P. Lukáš, M. Svoboda, Fatigue strength, microstructural stability and strain localization in ultrafine-grained copper, Mater. Sci. Eng. A 424 (2006) 97–104.
[22] H.W. Höppel, R.Z. Valiev, On the possibilities to enhance the fatigue properties of ultrafine-grained metals, Z. Metallk. 93 (2002) 641–648.
[23] M. Korn, R. Lapovok, A. Bohner, H.W. Höppel, H. Mughrabi, Bimodal grain size distributions in UFG materials produced by SPD - their evolution and effect on the fatigue and monotonic strength properties, Kovove Mater. 49 (2011) 51–63.
[24] T. Roland, D. Retraint, K. Lu, J. Lu, Fatigue life improvement through surface nanostructuring of stainless steel by means of surface mechanical attrition treatment, Scr. Mater. 54 (2006) 1949–1954.
[25] J.W. Tian, J.C. Villegas, W. Yuan, D. Fielden, L. Shaw, P.K. Liaw, D.L. Klarstrom, A study of the effect of nanostructured surface layers on the fatigue behaviors of a C-2000 superalloy, Mater. Sci. Eng. A 468 (2007) 164–170.
[26] H.W. Huang, Z.B. Wang, J. Lu, K. Lu, Fatigue behaviors of AISI 316L stainless steel with a gradient nanostructured surface layer, Acta Mater. 87 (2015) 150–160.
[27] J.Z. Long, Q.S. Pan, N.R. Tao, M. Dao, S. Suresh, L. Lu, Improved fatigue resistance of gradient nanograined Cu, Acta Mater. 166 (2019) 56–66.
[28] J.Z. Long, Q.S. Pan, N.R. Tao, L. Lu, Abnormal grain coarsening in cyclically deformed gradient nanograined Cu, Scr. Mater. 145 (2018) 99–103.
[29] L.J. Jing, Q.S. Pan, J.Z. Long, N.R. Tao, L. Lu, Effect of volume fraction of gradient nanograined layer on high-cycle fatigue behavior of Cu, Scr. Mater. 161 (2019) 74–77.
[30] L.J. Jing, Q.S. Pan, L. Lu, Effect of volume fraction of gradient nanograined layer on low-cycle fatigue behavior of Cu, Adv. Eng. Mater. 22 (2019) 1900554.
[31] T.H. Fang, W.L. Li, N.R. Tao, K. Lu, Revealing extraordinary intrinsic tensile plasticity in gradient nano-grained copper, Science 331 (2011) 1587–1590.
[32] S. Suresh, Fatigue of Materials, second ed., Cambridge University Press, Cambridge, 1998.
[33] J. Polák, M. Klesnil, Cyclic stress-strain response and dislocation structures in polycrystalline copper, Mater. Sci. Eng. 63 (1984) 189–196.
[34] Z.S. Basinski, S.J. Basinski, Fundamental aspects of low amplitude cyclic deformation in face-centred cubic crystals, Prog. Mater. Sci. 36 (1992) 89–148.
[35] H. Mughrabi, Cyclic hardening and saturation behavior of copper single-crystals, Mater. Sci. Eng. 33 (1978) 207–223.
[36] D.J. Morrison, V. Chopra, Cyclic stress-strain response of polycrystalline nickel, Mater. Sci. Eng. A 177 (1994) 29–42.
[37] C.E. Feltner, C. Laird, Cyclic stress-strain response of FCC metals and alloys 1. phenomenological experiments, Acta Metall. 15 (1967) 1621–1632.
[38] C.E. Feltner, C. Laird, Cyclic stress-strain response of F.C.C. metals and alloys–II Dislocation structures and mechanisms, Acta Metall. 15 (1967) 1633–1653.
[39] H. Mughrabi, Dislocation wall and cell structures and long-range internal stresses in deformed metal crystals, Acta Metall. 31 (1983) 1367–1379.
[40] P. Peralta, C. Laird, Fatigue of Metals, in: D.E. Laughlin, K. Hono (Eds.), Physical Metallurgy, (Fifth Ed.), Elsevier, Oxford, 2014, pp. 1765–1880.
[41] M.A. Meyers, K.K. Chawla, Mechanical Behavior of Materials, 2nd ed, Cambridge University Press, CambridgeUK, 2009.
[42] W. Chen, Z.S. You, N.R. Tao, Z.H. Jin, L. Lu, Mechanically-induced grain coarsening in gradient nano-grained copper, Acta Mater. 125 (2017) 255–264.
[43] X. Chen, Z. Han, X.Y. Li, K. Lu, Lowering coefficient of friction in Cu alloys with stable gradient nanostructures, Science Adv. 2 (2016) e1601942, 1–7.
[44] P.J.E. Forsyth, Exudation of material from slip bands at the surface of fatigued crystals of an aluminium copper alloy, Nature 171 (1953) 172–173.
[45] A.W. Thompson, W.A. Backofen, Effect of grain size on fatigue, Acta Metall. 19 (1971) 597–606.
[46] P. Lukáš, L. Kunz, Effect of grain-size on the high cycle fatigue behavior of polycrystalline copper, Mater. Sci. Eng. 85 (1987) 67–75.